A GNN-based Day Ahead Carbon Intensity Forecasting Model for Cross-Border Power Grids

Xiaoyang Zhang
The Hong Kong Polytechnic Univ.
xiaoyang.zhang@connect.polyu.hk

Dan Wang
The Hong Kong Polytechnic Univ.
dan.wang@polyu.edu.hk

ABSTRACT

Carbon intensity forecasting of power grids is critical to the optimization of demand-side consumers. Recently, *cross-border power grids* have emerged, i.e., those allowing electricity to be transmitted across different national transmission systems. Cross-border power grids substantially increase the sharing of highly variable renewable energy sources (VRE), leading to greater economic benefits and increased reliability. In Europe, the total volume of cross-border electricity that is exchanged comprises 13% of the annual net electricity that is generated. Current studies on carbon intensity forecasting, however, apply to individual regional power grids. In cross-border grids, the carbon intensity of a regional grid depends not only on that of its own electricity but also on the carbon intensity from the electricity exchanged with cross-border grids. Thus, if the cross-border electricity exchange is not captured appropriately, significant forecasting errors can occur.

In this paper, we formulate a new Carbon Intensity Forecasting for Cross-border Grids (CFCG) problem by proposing and integrating carbon flows generated by cross-border electricity exchanges. The challenge is to capture the complex spatial and temporal dependencies that are involved. We propose a CFCG model based on a Graph Neural Network (GNN) submodel to learn the spatial dependencies and a Long Short Term Memory (LSTM) submodel to learn the temporal dependencies. We evaluate the CFCG model using real-world data from the cross-border power grids in Europe involving 28 member countries. We compare five baseline models. Our results show that the CFCG model achieves an average improvement of 26.46% or 20.34% as compared to state-of-the-art forecasting models based on regional grids or one-hop neighbor grids, respectively.

CCS CONCEPTS

• **Computing methodologies** → **Neural networks**.

KEYWORDS

Cross-border Power Grids, Carbon Forecasting, Neural Networks

ACM Reference Format:
Xiaoyang Zhang and Dan Wang. 2023. A GNN-based Day Ahead Carbon Intensity Forecasting Model for Cross-Border Power Grids. In *The 14th ACM International Conference on Future Energy Systems (e-Energy '23), June 20–23, 2023, Orlando, FL, USA.* ACM, New York, NY, USA, 13 pages. https://doi.org/10.1145/3575813.3597346

e-Energy '23, June 20–23, 2023, Orlando, FL, USA

ACM ISBN 979-8-4007-0032-3/23/06…$15.00
https://doi.org/10.1145/3575813.3597346

1 INTRODUCTION

Global warming is attracting increasing attention in recent years [32, 38, 42]. Carbon emissions are a major factor in global warming [24]. Carbon emissions by the power sector increased by 700 Mt in 2021, accounting for 46% of the global increase [17]. There is a need for electricity generators and consumers alike to reduce their carbon usage.

Forecasting the carbon intensity of the electricity supplied by a power grid is critical in the optimization of demand-side consumers. Recently, *cross-border power grids* have emerged, i.e., those allowing electricity to be transmitted across the transmission systems of different countries. Cross-border power grids substantially increase the sharing of highly variable renewable energy sources (VRE), leading to greater economic benefits and increased reliability. In Europe, the total volume of cross-border electricity that is exchanged comprised 13% of the annual net electricity that is generated.

Current studies on carbon intensity forecasting apply to individual regional power grids. Forecasting models, e.g., Long Short Term Memory (LSTM), are trained on the historical data on the carbon intensity of a local regional grid, or in some recent studies on the carbon intensity of the one-hop neighbor grids is considered. In the context of cross-border power grids, when a consumer uses the electricity of a local grid, the carbon intensity of a local grid depends not only on that of the electricity of the local grid but also on the carbon intensity from the electricity exchanged with cross-border grids. For example, the carbon intensity of the local grids of Switzerland is small, yet, Switzerland imports electricity from Germany, Austria, Italy, and France. As such, carbon emissions are involved in the electricity supplied to consumers.

Clearly, if the cross-border electricity exchanges are ignored, significant forecasting errors can occur. We also observe that even if we estimate the carbon intensity using cross-border grids and then perform forecasting based on LSTM, non-trivial errors can still occur. Intrinsically, the historical trends in cross-border grids and the electricity that is exchanged in accordance with geographical topologies are dynamic and correlated across diverse granularities. It is, therefore, challenging to capture such correlations.

In this paper, we present a holistic study by formulating a new Carbon Intensity Forecasting for Cross-border Power Grids (CFCG) problem. In this problem, we propose cross-border carbon flows, and such flows form a carbon network. The challenge is to learn the complex spatial and temporal dependencies that are involved. We propose a new CFCG model based on Graph Neural Networks

(GNN) and LSTM.[1] Our model has three features: (1) the carbon intensity variation shows periodic patterns in multiple levels of granularity, e.g., hourly, daily, and weekly. To capture the patterns across various granularities, we develop a multi-periodic pattern encoding scheme to transform the original carbon intensity sequence data into data with different periodic granularity settings (e.g., hourly, daily, weekly); (2) Cross-border power grids have carbon flows with spatial dependencies. Thus, in our CFCG model, we develop and integrate a GNN-based submodel (i.e., GNN layers) to learn the spatial dependencies; (3) Carbon flows have time dependencies. Thus, in our CFCG model, we develop and integrate an LSTM-based submodel (i.e., LSTM layers) to uncover the temporal dependencies. Finally, to fuse different granularities, we generate the forecasting results using a Hadamard product.

We evaluate our model using the real-world dataset of the cross-border power grids of 28 countries in Europe. We evaluate CFCG with four state-of-the-art baseline schemes, including schemes using carbon intensity data from regional grids only, using data with one-hop neighbor grids. We also implement a forecasting scheme in which we apply the carbon intensity data of cross-border grids and we enhance it with forecasting capability by directly training an LSTM model; and we then compare CFCG to this model. Our evaluations show that our model can achieve an improvement of 26.46% and 20.34% as compared to two state-of-the-art schemes using regional grids or one-hop neighbor grids, respectively. As compared to a simple application of cross-border grids, we still see an improvement of 15.83%.

The contributions of the paper can be summarized as follows:

- We present a new study of carbon intensity forecasting in the context of cross-border power grids. We carefully analyze the literature and formulate a new carbon intensity forecasting problem, CFCG.
- We propose a CFCG model based on GNN and LSTM, where CFCG can uncover both spatial and temporal dependencies.
- We present an evaluation of CFCG using real-world data from the cross-border power grids of Europe, involving 28 countries. Our evaluation shows that CFCG outperforms state-of-the-art schemes, and that for certain countries, the improvement can be significant.

The remaining part of the paper proceeds as follows. In Section 2, we present the background on cross-border power grids, carbon emissions, and carbon intensity forecasting. We carefully analyze the related work and position our work in the literature. In Section 3, we present the problems of existing studies, and the need for a new study. This motivates our work. We formally formulate our CFCG problem in Section 4, and develop our solution model in Section 5. In Section 6, we evaluate our CFCG model, and we conclude our paper in Section 7.

2 BACKGROUND AND RELATED WORK

2.1 Cross-boarder Power Grids

Cross-border power grids [12, 26, 45] link two or more power grid systems, and allow electricity to be transmitted over larger areas across borders. There are three prominent advantages to cross-border power girds.

First, cross-border power grids help market participants to benefit from economies of scale on both the supply and demand sides. Larger generators can be operated to serve more consumers.

Second, cross-border power grids are diverse in terms of both supply and demand. This improves the security of the grids. For example, cross-border power grids can meet the peak demands with relatively fewer resources [25, 33].

Third, and increasingly important, is the environmental benefits of cross-border power grids. Cross-border power grids can integrate more variable renewables. On the one hand, they allow operators to leverage weather patterns across larger spaces. On the other hand, cross-border grids make it easier to balance the local variable renewable energy, as it can access greater supplies as well as additional pools of demands [5, 7].

Cross-border power grids are operated by joint operators. For example, the European Network of Transmission System Operators for Energy (ENTSO-E) operates the European cross-border power grids [41]. It was created to enhance cooperation between national power grid operators in Europe. The European cross-border power grids have expanded dramatically during over past years. According to the latest ENTSO-E statistic report [9], the volume of electricity that was exchanged was approximately 467TWh, comprising 13% of the net electricity that was generated. In 2022, 12 new borders received their first electric connectivity, joining 80 European borders [10]. Nine of the ENTSO-E member countries imported more than 50% of their total yearly electricity from their neighbors. Nearly 50% percent of the ENTSO-E member states imports and exports more than 20% of their domestic electricity generation from the cross-border power grid [14].

The intrinsic difference of a cross-border grid brings about as compared to a regional grid is that the carbon intensity borne by the grids involved a cross-border grid is calculated to reflect their state-level carbon intensity. Therefore, carbon intensity forecasting should carry this information.

2.2 Carbon Emission and Carbon Intensity Forecasting

In electricity generation, *carbon emissions* result from burning fuels in power plants. There are two types of carbon emissions [21]: (1) direct emissions, i.e., the operational carbon emissions that occur when the fuel is converted into electricity and (2) life-cycle emissions, which can be determined using methods of assessing life cycles [4, 16, 39].

The *carbon emission factor* (in g/kWh) is the quantity of carbon emitted per unit of electricity produced by a specific energy source (e.g., coal, wind, solar). Calculating the carbon emission factor is complex work and is beyond the scope of this paper. We take carbon emission factors as inputs. Table 1 shows the carbon emission factors for both direct emissions and life-cycle emissions [21]. The *carbon intensity* of a power grid is the carbon emission rate (in g/kWh) of this power grid, i.e., the total amount of carbon emitted (Gram) as against the electricity generated (Kilowatt-Hour). This can be calculated by the energy sources used in this power grid and the carbon emission factor of the energy sources. As compared

[1] We make our codes available: https://github.com/stuabc/CFCG

to the sheer amount of carbon emissions, carbon intensity is more commonly used as an index in making optimization decisions.

Carbon intensity forecasting aims to predict the carbon intensity of the electricity supplied by a power grid for a period of time in the future. It is useful for demand-side optimization, e.g., demand-side systems can switch their workloads to use electricity at a time that is "greener." For example, algorithms have been developed for smart home systems to enable the workloads of household appliances to be scheduled based on carbon intensity forecasting to reduce their carbon emissions [29]. Cloud computing schedules have been developed to distribute the workloads according to the carbon intensity at different times and places [28, 44]. In [3], deep learning model training schedules are based on carbon intensity forecasting.

2.3 Related Work

Estimating the Carbon intensity of a corporate entity has become an important problem with the increasing concerns over carbon emissions. Carbon intensity cannot be directly measured, but there are many ways to estimate carbon intensity. Below is a categorization of the related work. A summary is given in Table 2.

The related work can be grouped under the headings of *generation-based* carbon intensity estimation and *consumption-based* carbon intensity estimation. This follows the Greenhouse Gas (GHG) protocol [34] where the carbon emissions of a corporate entity are distinguished into (1) Scope 1, the emissions associated with the electricity generation of a corporate entity, e.g., burning fuels and (2) Scope 2, the emissions associated with the electricity consumed by a corporate entity [13]. [2] Generation-based estimation focuses on the calibration of carbon emission factors [23]. In particular, [39] calibrates the factors at an individual country level.

Our paper falls under the heading of consumption-based carbon intensity estimation. Consumption-based estimation can differ from generation-based estimation since a corporate entity, as an electricity consumer, can consume electricity generated from different power grids, e.g., through delivery by cross-border grids.

Research into consumption-based estimation can be further divided into *carbon intensity accounting* [36], i.e., to estimate the carbon intensity at a particular point in history or at the current time; and *carbon intensity forecasting*, i.e., to estimate the carbon intensity at a future time. Intrinsically, carbon intensity accounting is about trying to accurately estimate the ground truth; thus, it is useful for guiding financial investments, informing policy-making decisions, and measuring compliance with regulations [22]. The carbon intensity accounting of an individual regional grid is equivalent to generation-based carbon intensity estimation. To measure both the carbon generated in a regional grid and the carbon injected from networked grids, three recent schemes were developed [27, 31, 36]. All of these schemes calculate the injected carbon based on a proportional sharing principle, i.e., an equal distribution of the inflows. The difference is that (1) two schemes (direct coupling schemes) [27, 36] assume that each grid in the grid network is coupled with all other grids, with a difference in a weighting factor; and (2) one scheme (an aggregate coupling scheme) [31] assumes that the grid will firstly serve its own country, with the residual electricity available for use by other countries.

Our paper is about carbon intensity forecasting. As discussed, carbon intensity forecasting involves trying to accurately estimate carbon intensity at a future time; thus is useful for making decisions about demand-side optimization. Carbon intensity forecasting requires historical data on carbon intensity data and takes carbon intensity accounting as a building block for the ground truths. The technical difference between carbon intensity accounting and carbon intensity forecasting is that accounting is designed to calculate the ground truth at a point in history (or current) time; thus, the calculation uses the data in the *same* time slot. For forecasting, learning methods should be developed to learn the correlation within historical data across various time granularities.

There are carbon intensity forecasting schemes. Lowry, G. [19] proposed an algorithm to forecast the day-ahead carbon intensity of the power grids of the UK. Additional information was used to improve the forecasting results. For example, weather data were leveraged in [18] to forecast the carbon intensity of the power grids in Denmark. Recently, a scheme [21] developed a deep neural network (DNN) model for each energy source, e.g., coal, oil, solar, etc., and the carbon intensity forecasting of a regional grid is calculated by the average carbon intensity of all energy sources. Another study [20] focuses on multi-day carbon intensity forecasting, developing a hierarchical DNN model. As exchanges of electricity take place among cross-border grids, the carbon intensity of one-hop neighboring grids was considered in [18, 29] to improve the forecasting results. More specifically, the carbon intensity accounting takes one-hop neighbor grids into account when constructing historical and current carbon intensity data. Then, an LSTM model [29] or a hybrid model with linear regression, splines, and ARIMA [18] is used for forecasting. To the best of our knowledge, no existing study takes into consideration the electricity that is exchanged at the level of cross-border power grids. This paper fills in this gap.

We note that several commercial companies provide carbon intensity estimation services, e.g., ElectricityMap [35], Watttime [43]. Unfortunately, their models and data are not publically available.

3 MOTIVATION

In this section, we first show that carbon intensity accounting only using one-hop neighbor grids can deviate significantly from the ground truth with the full network of a cross-border grid. We then show that it is non-trivial to capture spatial information. More specifically, when applying an LSTM model to a state-of-the-art carbon intensity accounting scheme that takes into account the full networked grids, non-trivial forecasting errors can still occur.

We use the open data from ENSTON [37], which contains the electricity data of the power grids of 28 European countries from January 2019 to December 2021. Fig. 1 shows that the results of carbon intensity accounting when one-hop neighbor grids are used deviate from those when full networked grids are used. More specifically, we observe that 14 out of 28 countries have an error rate of 20% or higher and that 19 countries have an error rate of 10% or higher. The deviation can be significant in certain countries. For example, the carbon intensity of Sweden is 139.25g/kWh when we consider one-hop neighbor grids, yet it is 54.69g/kWh when we

[2] In GHG, there is a Scope 3, which includes all other emissions that occur in the upstream and downstream activities of a corporate entity. It is less related to this paper, and we do not discuss this category.

Table 1: Carbon emission factors (g/kWh) for different energy source

Emission factors	Oil	Coal	Natural gas	Nuclear	Wind	Solar	Hydro	Geothermal	Biomass	Other
Direct emissions	406	760	370	0	0	0	0	0	0	575
Life-cycle emissions	650	820	490	12	11	45	24	38	230	700

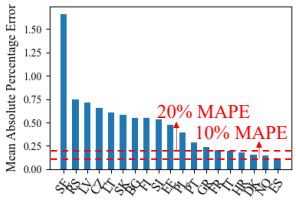

Figure 1: The countries with an accounting error over 10%.

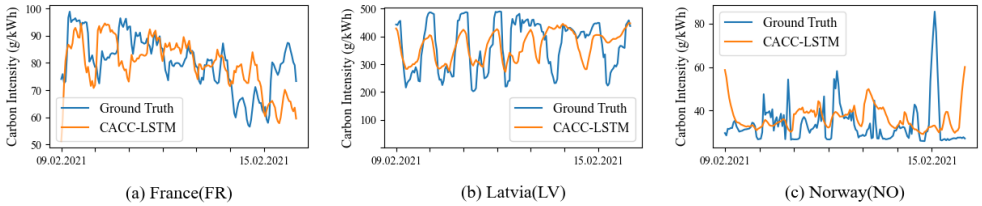

(a) France(FR) (b) Latvia(LV) (c) Norway(NO)

Figure 2: The forecasting performance of CACC-LSTM

Table 2: Research summary on Carbon Intensity Estimation

Generation-based Carbon Intensity Estimation	Consumption-based Carbon Intensity Estimation		
[1] [2] [8]	Carbon Intensity Accounting	[27][31] [36]	
	Carbon Intensity Forecasting	Regional grids	[6] [19][20][21]
		One-hop neighbor grids	[18][29]
		Cross-border grids	CFCG

consider full networked grids, a difference of 165.67%. When we look into the data, we observe that Denmark, a one-hop neighbor grid of Sweden has high carbon intensity in its electricity, leading to a high carbon intensity when considering one-hop neighbor grids.

We then study whether a simple carbon intensity forecasting scheme based on carbon intensity accounting with networked grids can have good performance. We apply the state-of-the-art Carbon intensity ACCounting scheme [36] (we call it CACC in this paper) and we enhance it with forecasting capability by training an LSTM model using the historical carbon intensity data of CACC. In this paper, we call this approach CACC-LSTM.[3] We divide the ENSTON data into training data (60%), validation data (20%), and testing data (20%). We show the carbon intensity (g/KWh) in the first week of the testing data, i.e., February 9^{th} 2021 to February 15^{th} 2021.

We easily find that the forecasting results of a number of countries display non-trivial errors. Fig. 2 shows the results of the CACC-LSTM of France, Latvia, and Norway, where the errors are 12.12%, 16.69%, and 21.11%, respectively. As was explained, CACC was designed to calculate the carbon intensity at a point of time in history (or currently) time using the data of the *same* time slot. As such, CACC-LSTM lacks the ability to fully capture the dynamics and correlation across diverse granularities, e.g., hourly, daily, and weekly. Overall, there are challenges to capturing the correlations across diverse granularity periods, to capturing both spatial and temporal correlations, and to fusing models if submodels are needed. This motivated us to present a holistic study by formulating a new problem and developing a new forecasting model.

[3]CACC-LSTM is intrinsically equivalent to enhancing [29] where we extend its carbon intensity accounting from one-hop neighbor grids to networked grids.

4 PROBLEM STATEMENT

4.1 Carbon Network Modeling

Let i and j be two power grids. The *electricity flow* $f^e_{ij}(t)$ is the total amount of electricity transmitted from i to j during a period of time starting at t. In practice, the time period is one hour. Let $E_i(t)$ be the electricity generated by power grid i at time t. This electricity is an aggregation of the electricity generated by different energy sources, e.g., Oil, Coal, Wind, Biomass, etc. Let $\mathcal{S}$ be the set of energy sources and $S = |\mathcal{S}|$. Let $E^k_i(t)$ be the electricity generated by source k at power grid i. Clearly $E_i(t) = \sum_{k\in\mathcal{S}} E^k_i(t)$.

As was mentioned, different energy sources are used to generate electricity, and the carbon emitted by each type of energy source differs. Let ef^k be the *carbon emission factor* of an energy source k. In this paper, we take this carbon emission factor as a constant for a specific energy source [21]. For example, the carbon emission factor of Oil is 406g/kWh and the carbon emission factor of Wind is 0. We show the most common energy sources used to generate electricity and their carbon emission factor in Table 1.

At a specific time t, a power grid i generates electricity using different energy sources: this is because the amount of certain energy sources change at different times, e.g., solar, wind, etc. This leads to dynamic carbon emissions at different times. Let *carbon intensity* $ci(t)$ be the ratio of the total carbon emissions as against the total electricity generated. Specifically,

$$ci(t) = \frac{\sum_{k\in\mathcal{S}} ef^k \times E^k(t)}{E(t)} \quad (1)$$

Note that carbon intensity cannot be directly measured. It is calculated using Eq. 1.

In practice, two grids can exchange electricity when they have connecting lines for electricity transmissions. We call them *neighboring grids*. Note that when a grid i receives electricity flow f^e_{ij} from grid j, i also bears the carbon generated by this electricity flow. We call this *carbon flow*. Intuitively, we can think that the carbon emission "flows" from grid i to j. Let carbon flow $f^c_{ij}(t)$ be the total amount of carbon generated by the electricity flow $f^e_{ij}(t)$ at time t. More specifically, this is the amount of carbon associated

with the electricity generated by grid i and transmitted to grid j at t. $f^c_{ij}(t) = f^e_{ij}(t) \times ci_i(t)$.

Below, we formally present the carbon network modeling formally in the following. For clarity, we summarize key notations in Table 3.

Table 3: Notations and Descriptions.

Notations	Descriptions
$\mathcal{G} = (\mathcal{V}, \mathcal{E}, \mathcal{A})$	Directed graph representing carbon network
$ci_i(t)$	Carbon intensity of power grid i at time t
$\boldsymbol{ci}(t) = \{ci_i(t)\} \in \mathbb{R}^{\mathcal{V}}$	Carbon intensity of all power grids at time t
$\boldsymbol{CI} = \{\boldsymbol{ci}(0), ..., \boldsymbol{ci}(t)\}$	Carbon intensity sequence of all power grids
$f^e_{ij}(t)$	Electricity flow from grid i to grid j at time t
$\boldsymbol{f^e}(t) = \{f^e_{ij}(t)\} \in \mathbb{R}^{\mathcal{E}}$	Electricity flows of all power grids at time t
$\boldsymbol{F^e} = \{\boldsymbol{f^e}(0), ..., \boldsymbol{f^e}(t)\}$	Electricity flow sequence of all power grids

Definition 1. ***Carbon network.*** *We use a directed graph $\mathcal{G} = (\mathcal{V}, \mathcal{E}, \mathcal{A})$ to represent a carbon network where $\mathcal{V} = v_1, ..., v_n$ is a set of nodes, v_i denotes a regional power grid, and $|\mathcal{V}| = n$. $\mathcal{E}$ is a set of links, where directed link (v_i, v_j) indicates that grid v_j will directly import electricity from grid v_i. We use a binary adjacency matrix $\mathcal{A} \in \mathbb{R}^{n \times n}$ to present the connectivity among the power grids.*

We now introduce two features that are useful for our learning model: (1) the carbon intensity sequence, a feature on nodes; and (2) the electricity flow sequence, a feature on links. The history carbon intensity sequence data and electricity flow sequence data are the inputs of our learning model.

Definition 2. ***Carbon intensity sequence.*** *Recall that $ci_i(t)$ is the carbon intensity of a power grid i at time t. We denote the carbon intensity sequence of i as a vector $\boldsymbol{ci}(t) = \{ci(0), ..., ci(t)\} \in \mathbb{R}^{\mathcal{V}}$. This is a time series data. The carbon intensity sequence of all power grids at time t is denoted as a matrix $\boldsymbol{CI} = \{\boldsymbol{ci}(t)\}$.*

Definition 3. ***Electricity flow sequence.*** *Recall that $f^e_{ij}(t)$ is the electricity flow from power grid i to j at time t. We denote the all electricity flows of a carbon network at time t as a matrix $\boldsymbol{f^e}(t) = \{\forall i, j, f^e_{ij}(t)\} \in \mathbb{R}^{\mathcal{E}}$. The electricity flow sequence of a carbon network over a period of time t is denoted as a three-dimensional matrix $\boldsymbol{F^e} = \{\boldsymbol{f^e}(0), ..., \boldsymbol{f^e}(t)\}$.*

The carbon intensity sequence is a two-dimensional matrix since it is on a node i, yet the electricity flow sequence is a three-dimensional matrix since it works on a link (i, j).

4.2 Problem formulation

Problem CFCG (**C**arbon intensity **F**orecasting for **C**ross-border power **G**rids): Given the carbon network $\mathcal{G} = (\mathcal{V}, \mathcal{E}, \mathcal{A})$, historical carbon intensity sequence $\boldsymbol{CI} = \{(\boldsymbol{ci}(0), ..., \boldsymbol{ci}(t)\}$, historical electricity flow sequence $\boldsymbol{F^e} = \{\boldsymbol{f^e}(0), ..., \boldsymbol{f^e}(t)\}$, learn a predictive function $y = f(\mathcal{G}, \boldsymbol{CI}, \boldsymbol{F^e})$, which infers the day-ahead carbon intensity sequence of cross-border power grids.

5 A GNN-LSTM-BASED CFCG MODEL

5.1 Overview

We developed a new CFCG model, see Fig. 3. CFCG consists of four components. First, to capture the dynamics across diverse periods, CFCG divides the data into multiple periods, i.e., hourly, daily, and weekly. In our experiments, we will evaluate the granularity of the periods. CFCG has a multi-periodic pattern encoding component to perform a granularity-aware encoding on the input data. Second, to learn spatial dependencies, CFCG adopts a GNN layer with a specific embedding mechanism. Third, to learn the temporal dependencies, CFCG adopts an LSTM layer to take the embedding generated by the GNN layer as inputs, and outputs a high-level representation. Fourth, to integrate the outputs and generate the forecasting results, CFCG fuses the outputs of the LSTM layer using a Hadamard product.

5.2 Multi-periodic Pattern Encoding

The carbon intensity variation has multi-periodic patterns [21]. We propose to leverage multiple time granularites (e.g., hourly, daily, and weekly) to model the temporal patterns. Similar techniques have been used to predict city traffic [46, 47]. Specifically, each time granularity is regarded as a period to sample the carbon intensity data points. We can then generate a set of granularity-specific data series. We define *granularity-aware carbon intensity sequence* and *granularity-aware electricity flow sequence.*

Definition 4. ***Granularity-aware Carbon Intensity Sequence.*** *Let $\boldsymbol{CI^p} \in \mathbb{R}^{N \times T_p}$ be a granularity-specific carbon intensity sequence with a period granularity of p (e.g., an hour), where N is the number of power grids, and T_p is the length of the carbon intensity series under p.*

For example, when $p = day$, T_p is 24 times that of $p = hour$.

$$\boldsymbol{CI^p} = \{\boldsymbol{ci^p}(0), ..., \boldsymbol{ci^p}(t-1), \boldsymbol{ci^p}(t), \boldsymbol{ci^p}(t+1), ..., \boldsymbol{ci^p}(T_p)\}(p = hour)$$

$$\boldsymbol{CI^p} = \{\boldsymbol{ci^p}(0), ..., \boldsymbol{ci^p}(t-24), \boldsymbol{ci^p}(t), \boldsymbol{ci^p}(t+24), ..., \boldsymbol{ci^p}(T_p)\}(p = day)$$

Similarly, the granularity-aware electricity flow sequence is:

Definition 5. ***Granularity-aware Electricity Flow Sequence*** *Let $\boldsymbol{F^{e,p}} \in \mathbb{R}^{M \times T_p}$ be a granularity-specific electricity flow sequence with the period granularity of p (e.g., an hour), where M is the number of links, and T_p is the length of the carbon intensity series under p.*

In this component, the multi-periodic pattern encoding takes the granularity period p, the historical data of the carbon intensity sequence, and the electricity flow sequence as inputs and outputs the granularity-aware carbon intensity sequence and the granularity-aware electricity flow sequence.

5.3 GNN-based Spatial Dependency Learning

The spatial dependency of the carbon intensity of the nodes and the spatial dependency of the electricity flows of the links are key characteristics of the CFCG problem. We develop a GNN layer based on graph attention networks [40] to capture such spatial dependencies.

In the carbon network, nodes have physical restrictions. For example, certain nodes only serve as exporters. If we treat all nodes

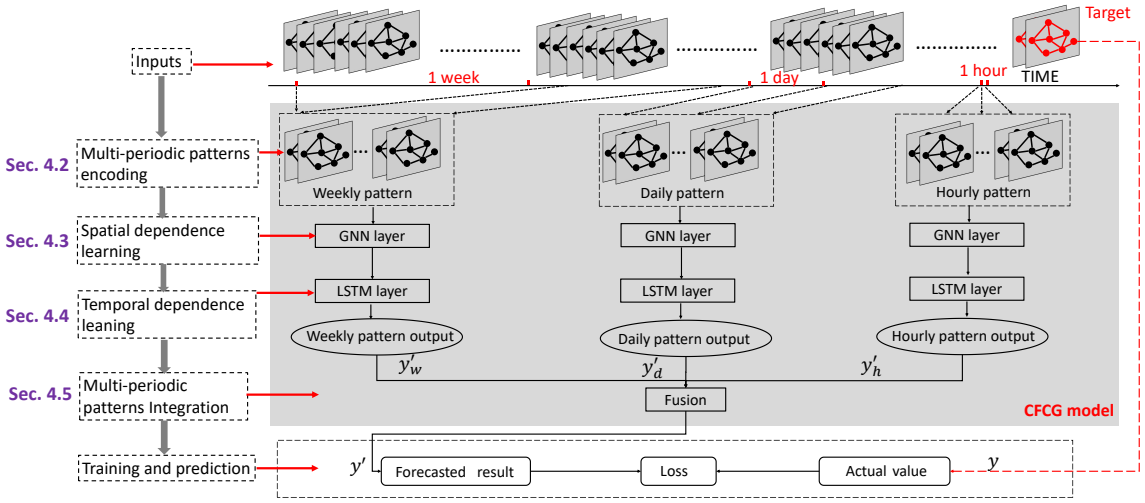

Figure 3: Overview. We take the history carbon intensity sequence and electricity flow sequence as input and obtain the final prediction result through our CFCG model.

as the same in the GNN layer, we observe that there can be noises. As such, we develop a node-aware embedding mechanism with a set of rules. Such embedding can effectively remove noises.

More specifically, we summarize three simple rules:

- The carbon intensity of a grid serving only as an exporter will not be affected by neighboring grids..
- The carbon intensity of a grid serving only as an importer will be affected by all neighboring grids.
- The carbon intensity of a grid serving as both importer and exporter will be affected by the neighboring grids that export electricity to it.

Note that in a GNN iteration, there is a node embedding operation. More specifically, each node will aggregate the features (i.e., carbon intensity sequence and electricity flow sequence) of neighbor nodes by using learnable normalized attention weights. As such, (Related to rule 1) For a node that is serving as only an exporter, its embedding is based on itself; (Related to rule 2) For a node that is serving as only an importer, its embedding is generated by aggregating the features of all neighboring nodes, links, and corresponding weight; and (Related to rule 3) For a node that is serving as both importer and exporter, its embedding is generated based on the features of neighboring nodes, links, and corresponding weights except for the neighboring nodes that import from it and related flows. Fig. 4 shows an example of the node embedding process, where α is a learnable weight coefficient.

We would first like to briefly present the node embedding operation. We leverage attention mechanism [40] to learn the node embedding. Specifically, for each node i, the node embedding is generated by the features aggregated from the neighboring nodes and edges with corresponding weights. Let $\mathcal{N}_i^{all}$ and $\mathcal{E}_i^{all}$ be the set of nodes and edges connected to node i, respectively; in particularly, node i is included in $\mathcal{N}_i^{all}$. For each node i, the neighboring nodes set $\mathcal{N}_i \subseteq \mathcal{N}_i^{all}$ and neighboring edges set $\mathcal{E}_i \subseteq \mathcal{E}_i^{all}$ are different when they conform to different rules. We first introduce the neighboring nodes and edges definition for each rule. Then we demonstrate the node embedding calculation process based on the defined neighboring nodes and edges.

For a node i that conforms to Rule 1, the node embedding is calculated based on the exporter itself, and only the feature of the exporter contributes to the embedding. Thus, we have the neighboring nodes set $\mathcal{N}_i = \{i\}$ and the neighboring edges set $\mathcal{E}_i = \emptyset$.

For a node i that conforms to Rule 2, the node embedding is calculated based on all the nodes and edges connected to it. Thus, we have the neighboring nodes set $\mathcal{N}_i = \mathcal{N}_i^{all}$ and the neighboring edges set $\mathcal{E}_i = \mathcal{E}_i^{all}$.

For a node i that conforms to Rule 3, the node embedding is calculated based only on nodes and edges that export to it. Thus, we have the neighboring nodes set $\mathcal{N}_i \subset \mathcal{N}_i^{all}$ and the neighboring edges set $\mathcal{E}_i \subset \mathcal{E}_i^{all}$.

With the neighboring nodes $\mathcal{N}_i$ and neighboring edges E_i now defined, we can derive the node embedding based on the embedding weights that are widely used in graph attention networks [40]. Specifically, we suppose that there are N_i neighboring nodes and E_i neighboring edges for each node i. Let $\mathbf{ci}_i^p(t) = \{ci_1^p(t), \ldots, ci_{N_i}^p(t)\}$ and $\mathbf{f}_i^{e,p}(t) = \{f_1^{e,p}(t), \ldots, f_{E_i}^{e,p}(t)\}$ be the set of neighboring node features and edge features, respectively. For each node i, the embedding weight $\alpha_{ij}^n(t)$ is defined as follows:

$$\alpha_{ij}^n(t) = \frac{exp(\sigma(a_n^T[W_n ci_i^p(t) \| W_n ci_j^p(t)]))}{\sum_{k \in \mathcal{N}_i} exp(\sigma(a_n^T[W_n ci_i^p(t) \| W_n ci_k^p(t)]))}, \quad (2)$$

where W_n is a learnable weight matrix that linearly transforms the node features into high-level features, a_n is the parameter vector of a feed-forward network with a single layer, and σ represents the activation function. Similarly, the embedding weight of edge $k \in \mathcal{E}_i$ to node i is defined as $\alpha_{ik}^e(t)$, and we have:

$$\alpha_{ik}^e(t) = \frac{exp(\sigma(a_e^T[W_n ci_i^p(t) \| W_e f_j^{e,p}(t)]))}{\sum_{j \in \mathcal{E}_i} exp(\sigma(a_e^T[W_n ci_i^p(t) \| W_e f_j^{e,p}(t)]))}, \quad (3)$$

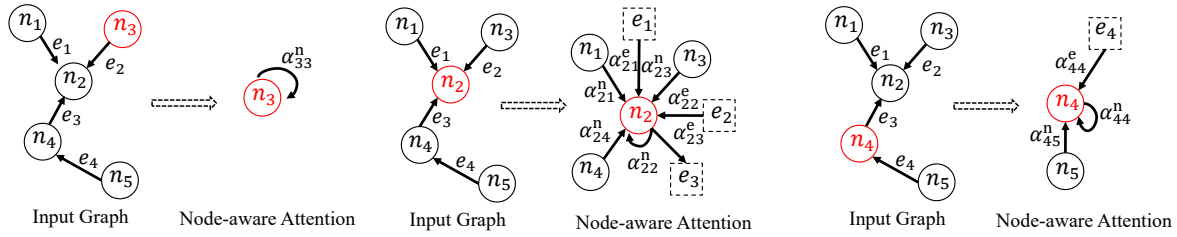

(a) Node serves only as an exporter (b) Node serves only as importer (c) Node serving as both exporter and importer

Figure 4: (a) Illustration of the node-aware embedding of node n_3. The embedding generation for a node serving as only as an exporter is based on itself. (b) Illustration of the node-aware embedding of node n_2. The embedding generation for a node serving as only an importer is based on all neighboring nodes and edges. (c) Illustration of the node-aware embedding of node n_4. The embedding generation for a node serving as both importer and exporter is based on information from neighboring nodes and edges that export to it.

where W_e is a learnable weight matrix that linearly transforms the edge features into high-level features, and a_e is the parameter vector of a feed-forward network with a single layer.

With the embedding weights $\alpha^n_{ij}(t)$ and $\alpha^e_{ik}(t)$ learned, we can derive the node embedding of node i, which is the concatenation of the weighted neighboring nodes feature and edges features. Let $\tilde{ci}^p_{\mathcal{N}_i}(t)$ and $\tilde{ci}^p_{\mathcal{E}_i}(t)$ be the weighted sum of neighboring nodes and edge features. We then have:

$$\tilde{ci}^p_{\mathcal{N}_i}(t) = \sigma(W_n \cdot \sum_{j \in \mathcal{N}_i} \alpha^n_{ij}(t) ci^p_j(t)), \tag{4}$$

and

$$\tilde{ci}^p_{\mathcal{E}_i}(t) = \sigma(W_e \cdot \sum_{k \in \mathcal{E}_i} \alpha^e_{ij}(t) f^{e,p}_k(t)). \tag{5}$$

Finally, the node embedding $\tilde{ci}^p_i(t)$ of node i can be combined by a concatenation operation $\|$:

$$\tilde{ci}^p_i(t) = (\tilde{ci}^p_{\mathcal{N}_i}(t) \| \tilde{ci}^p_{\mathcal{E}_i}(t)) \tag{6}$$

5.4 LSTM-based Temporal Dependence Learning

Spatial dependency learning provides the representation of each node integrated with the representation of the nodes and links in the carbon network. We next learn the temporal dependency. We leverage LSTM [15], a neural network that can successfully process time series data, to learn the temporal dependency. Specifically, there is a memory cell $\mathbf{c}_t$ to store the observation of time step t, and three gates are designed to control the state of the memory cell: forget gate $\mathbf{f}_t$, input gate $\mathbf{i}_t$ and output gate $\mathbf{o}_t$. Let $\mathbf{x}_t$ be the input, and the LSTM function $LSTM(\mathbf{x}_t)$ can be defined as:s

$$LSTM(\mathbf{x}_t) = \mathbf{o}_t \odot \phi(\mathbf{c}_t), \tag{7}$$

where $\phi(\cdot)$ is a tangent function, $\mathbf{c}_t = \mathbf{f}_t \odot \mathbf{c}_{t-1} + \mathbf{i}_t \odot \mathbf{c}_t$, and $\odot$ denotes the operation of product.

For the hourly carbon intensity sequence, the input of the LSTM network is defined as $\widetilde{\mathbf{CI}}_h = \{\widetilde{\mathbf{ci}}^p(0), \ldots, \widetilde{\mathbf{ci}}^p(t), \widetilde{\mathbf{ci}}^p(t+1), \ldots, \widetilde{\mathbf{ci}}^p(T_p)\}$. The output of the LSTM network is defined as

$$y'_h = LSTM(\widetilde{\mathbf{CI}}_h) \tag{8}$$

For the daily carbon intensity sequence, the input of the LSTM network is defined as $\widetilde{\mathbf{CI}}_d = \{\widetilde{\mathbf{ci}}^p(0), \ldots, \widetilde{\mathbf{ci}}^p(t), \widetilde{\mathbf{ci}}^p(t+24), \ldots, \widetilde{\mathbf{ci}}^p(T_p)\}$. The output of the LSTM network is defined as

$$y'_d = LSTM(\widetilde{\mathbf{CI}}_d) \tag{9}$$

For the weekly carbon intensity sequence, the input of the LSTM network is defined as $\widetilde{\mathbf{CI}}_w = \{\widetilde{\mathbf{ci}}^p(0), \ldots, \widetilde{\mathbf{ci}}^p(t), \widetilde{\mathbf{ci}}^p(t+168), \ldots, \widetilde{\mathbf{ci}}^p(T_p)\}$. The output of the LSTM network is defined as

$$y'_w = LSTM(\widetilde{\mathbf{CI}}_w) \tag{10}$$

5.5 Multi-periodic patterns Integration

In this part, we will discuss how to generate the final prediction result. We develop a gating mechanism [11] to fuse representations with different granularites. Specifically, we generate the final prediction result Y' by the Hadamard product $\odot$. After learning the temporal dependence of carbon intensity with LSTM, we can obtain the predicted future carbon intensity in three granularities: hourly representation y'_h, daily representation y'_d, and weekly representation y'_w. Then, we can integrate them to obtain the final prediction result as follows:

$$Y' = W_h \odot y'_h + W_d \odot y'_d + W_w \odot y'_w \tag{11}$$

where W_h, W_d, and W_w are learnable parameters for different granularity-aware representations, reflecting the weight of the three components on the forecasting target.

6 EVALUATION

6.1 Evaluation Setup

In this section, we present the evaluation of our CFCG model with the following research questions.

RQ1: How does CFCG perform when compared with state-of-the-art day-ahead carbon intensity forecasting techniques?

RQ2: How do our designs in the key components contribute to the performance of CFCG?

RQ3: What explainable patterns does CFCG capture during carbon intensity forecasting?

RQ4: The CFCG model applies a carbon intensity accounting method as a building block. How does the carbon intensity accounting component affect our CFCG model?

Table 4: Performance comparison of all approaches on datasets of 28 countries in terms of MAE, RMSE, and MAPE (based on lifecycle emission factors).

Methods	Metric	Countries														
		AT	BE	BG	CH	CY	CZ	DE	DK	EE	ES	FI	FR	GR	HR	HU
DACF	MAE	36.02	34.68	20.95	110.25	**20.64**	32.60	39.16	45.77	68.74	25.16	12.55	9.50	**39.43**	34.30	20.99
	RMSE	48.82	43.28	27.01	143.56	**27.89**	39.80	54.94	57.40	86.00	32.57	17.38	12.92	**52.91**	43.20	26.45
	MAPE(%)	24.07	19.61	5.53	59.06	**3.44**	8.00	11.31	25.20	25.33	14.95	10.21	18.77	**11.37**	14.43	9.10
TSBP	MAE	24.02	27.34	23.42	60.7	20.8	27.32	42.39	36.77	40.3	27.87	16.02	8.96	47.44	34.28	21.13
	RMSE	32.32	34.82	29.57	81.15	27.96	34.52	55.02	46.68	53.54	35.41	20.43	12.06	59.47	42.42	26.41
	MAPE(%)	17.83	15.16	4.90	45.49	3.97	6.01	11.58	18.53	13.17	14.44	12.75	16.50	11.73	12.75	7.51
HCMF	MAE	23.92	28.73	26.93	65.62	21.88	27.38	47.81	37.27	42.75	28.12	16.00	9.35	55.68	34.71	22.23
	RMSE	32.57	35.91	33.75	86.79	28.94	34.72	59.54	47.04	54.38	35.72	20.94	12.38	67.69	42.91	27.66
	MAPE(%)	16.58	15.85	5.86	46.85	3.65	6.12	12.76	18.37	13.87	14.16	11.54	16.94	13.21	12.43	7.51
CCAC	MAE	25.93	32.42	20.82	49.57	27.34	26.01	51.45	44.94	45.96	26.78	13.16	9.56	53.09	25.71	19.37
	RMSE	36.34	42.42	28.20	51.20	41.20	35.13	68.38	58.71	63.74	34.90	18.70	13.23	70.26	34.15	25.25
	MAPE(%)	18.82	18.45	5.64	44.52	4.64	6.82	17.09	23.54	16.73	16.89	10.04	18.40	15.11	11.67	8.43
CCAC-LSTM	MAE	24.13	28.56	23.88	45.90	21.94	25.48	46.78	36.22	36.82	26.55	12.46	9.19	45.29	28.38	21.53
	RMSE	32.53	35.77	30.42	81.88	28.89	32.99	58.96	45.91	50.73	33.78	16.96	12.12	59.19	36.15	27.24
	MAPE(%)	19.13	17.69	5.46	40.62	3.66	6.57	14.60	19.46	12.99	15.82	10.65	18.75	13.22	11.67	9.49
CFCG	MAE	**22.92**	**26.21**	**19.27**	**28.16**	23.26	**23.05**	**38.51**	**34.57**	**35.24**	**19.94**	**11.71**	**7.96**	41.72	**23.40**	**16.33**
	RMSE	**31.93**	**34.54**	**25.66**	**39.37**	32.61	**30.37**	**54.79**	**44.82**	**49.95**	**26.84**	**15.97**	**11.16**	55.21	**31.05**	**21.19**
	MAPE(%)	**16.57**	**15.05**	**4.75**	**29.70**	3.93	**5.97**	**10.91**	**16.94**	**12.48**	**12.67**	**8.86**	**14.74**	11.56	**10.34**	**7.06**

Methods	Metric	Countries													
		IE	IT	LT	LV	NL	NO	PL	PT	RS	RO	SE	SI	SK	AVERAGE
DACF	MAE	**53.59**	26.43	74.14	58.71	33.31	10.11	41.63	40.06	36.48	30.28	6.80	40.21	45.00	37.41
	RMSE	**76.12**	33.72	91.65	73.99	45.44	19.42	51.79	52.24	47.12	39.40	8.97	48.17	52.86	48.39
	MAPE(%)	**16.03**	8.50	46.95	24.66	7.11	20.81	6.57	23.88	7.38	9.42	12.89	31.09	16.17	17.57
TSBP	MAE	84.27	27.76	62.67	76.76	32.09	10.11	38.6	40.93	49.11	32.12	10.13	40.96	26.33	35.38
	RMSE	106.76	34.56	78.68	91.81	43.91	17.07	49.56	52.49	60.34	40.97	12.91	51.22	32.97	45.15
	MAPE(%)	24.13	7.37	39.35	31.52	7.06	23.13	5.71	22.89	7.83	9.46	19.35	22.50	9.29	15.78
HCMF	MAE	88.24	28.29	64.85	75.80	33.37	10.43	39.92	40.14	64.12	33.61	10.17	43.23	27.68	37.44
	RMSE	109.81	35.68	80.79	91.07	44.80	17.05	50.67	53.89	80.62	42.72	12.80	52.29	34.41	47.34
	MAPE(%)	24.64	7.48	41.50	30.96	7.08	23.53	5.79	22.76	11.41	9.57	19.05	25.42	9.37	16.22
CCAC	MAE	106.44	23.32	61.50	44.97	42.69	9.52	45.92	49.09	33.94	35.78	5.85	24.94	24.08	35.01
	RMSE	139.95	30.59	86.36	61.13	57.18	19.76	61.70	65.30	44.93	47.17	8.50	34.06	31.71	46.79
	MAPE(%)	35.79	7.92	36.77	19.53	9.05	22.42	7.52	30.91	6.84	11.70	10.60	15.02	9.72	16.44
CCAC-LSTM	MAE	90.84	23.46	60.30	44.77	33.50	9.32	39.29	40.68	37.67	33.38	7.06	26.45	24.71	32.88
	RMSE	111.70	30.08	77.70	58.01	44.83	17.10	49.99	52.35	48.13	42.19	9.27	33.15	31.39	42.48
	MAPE(%)	27.09	7.80	36.17	18.06	7.11	21.23	6.34	25.23	7.55	10.26	13.97	19.67	9.43	15.35
CFCG	MAE	84.10	**20.67**	**51.96**	**39.33**	**32.09**	**8.38**	**34.45**	**37.26**	**32.83**	**29.28**	**5.34**	**22.28**	**23.09**	**28.33**
	RMSE	98.02	**26.64**	**69.67**	**52.09**	**43.70**	**15.85**	**45.87**	**50.18**	**43.13**	**38.63**	**7.56**	**29.59**	**29.68**	**37.72**
	MAPE(%)	22.66	**6.97**	**29.30**	**17.47**	**6.95**	**19.89**	**5.61**	**22.74**	**6.76**	**9.40**	**9.64**	**13.68**	**9.22**	**12.92**

Data Description. To evaluate the performance of CFCG, we use the real-world electricity dataset from the cross-border power grids of the European Network of Transmission System Operators for Electricity's (ENTSOE's) transparency platform [37]. The data is comprised of hourly electricity production data and cross-border electricity flow data from 2019 to 2021. The data of 28 countries are included. For the sake of brevity, we present the abbreviation of countries in Append A.

Evaluation Metrics. We adopt three commonly used metrics: (1) *Mean absolute error (MAE)*: $MAE = \frac{1}{m}\sum_i^m |y_i - y_i'|$. (2) *Mean Absolute Percentage Error (MAPE)*: $MAPE = \frac{1}{m}\sum_i^m \left|\frac{y_i - y_i'}{y_i}\right|$. (3) *Root Mean Squared Error (RMSE)*: $RMSE = \sqrt{\frac{1}{m}\sum_i^m |y_i - y_i'|}$.

Carbon Intensity Ground Truth. As discussed, the carbon intensity cannot be directly measured. Different carbon intensity accounting methods are used to estimate the ground truth of carbon intensity. In this paper, we apply three methods[27, 31, 36]. We use [27] as our baseline ground truth and we show its detailed computation in Appendix B. We will evaluate the impact of different ground truths on our CFCG model.

Training and Testing. We use the first 60% of the data as the training set, the next 20 as the validation set, and the remaining 20% as the test set. Our model is trained using the RMSprop Optimizer [30]. To prevent overfitting, we employ early-stopping and model checkpointing techniques. To maintain the forecasting accuracy, we re-train our model every three months.

Baselines. We compare our CFCG model with the following:

DACF [21]: DACF is a state-of-the-art forecasting scheme for regional grids. DACF establishes a DNN model for each energy source and then calculates the averaged carbon intensity. It does not consider spatial dependencies to forecasts for regional grids.

TSBP [29] and *HCFM* [18]: TSBP and HCFM are schemes that estimate the historical and current carbon intensities using one-hop carbon intensity accounting. Then TSBP then applies an LSTM model to forecast the carbon intensity of the grid, whereas HCFM develops a hybrid model based on linear regression, splines, and ARIMA to forecast the carbon intensity of the grid.

CACC and *CCAC-LSTM*: CCAC is the carbon intensity accounting scheme in [36]. We use the carbon intensity of the current time as the forecasting result of the next time slot. CCAC-LSTM (described in Section 3) enhances CACC with an LSTM model, i.e., the LSTM model will be trained by being given the historical carbon data of CACC.

6.2 Performance Results (RQ1)

We compare the performance of CFCG with five baselines. Table 4 shows the results in terms of MAE, RMSE, and MAPE, where the best-performing method is highlighted in bold font.

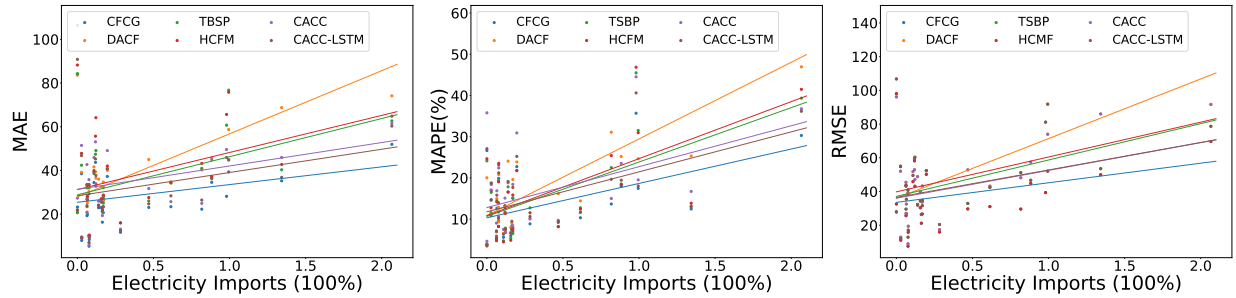

Figure 5: The points in the scatter plot represent the performance of each model on the countries. Forecast errors are higher in countries with larger proportions of electricity imports and generation.

Overall, CFCG outperforms existing schemes DACF, TSBP, HCMF, and CCAC by at least 18.12%. More specifically, CFCG achieves an average improvement of 26.46% (from 17.57% to 12.92%), 18.12% (from 15.78% to 12.92%), 20.34% (from 16.22% to 12.92%), and 21.41% (from 16.44% to 12.92%) in MAPE. Even compared to CCAC-LSTM, we see an improvement of 15.83% (from 15.35% to 12.92%). On average, CFCG not only outperforms previous models, but we also observe that CFCG outperforms TSBP, HCMF, CACC, and CCAC-LSTM in all countries. The only exception is that DACF outperforms CFCG in Cyprus, Ireland, and Greece, where regional grids dominate. CFCG inherits the features of existing models and captures new features. Thus, CFCG can steadily outperform other models.

Fig. 5 shows forecasting errors as a function of the ratio of electricity imports (0 to over 200%). Each dot represents a country and different countries have different import ratios. We see that forecasting errors increase as electricity imports increase. This is because the difficulty of forecasting increases when more dynamics are involved. We can also see that our CFCG model not only outperforms all other schemes, but that our errors also increase more slowly in comparison to the increase in the electricity import ratios. DACF, TBSP, and HCFM perform better than CACC and CACC-LSTM when the electricity import ratio is small. Clearly, these schemes perform well when a regional grid dominates. When the electricity import ratio increases, the performance of CACC and CACC-LSTM improves.

6.3 Model Ablation Study (RQ2)

We now evaluate our designs in two key components of CFCG through an ablation study, the granularity-aware encoding component and the node-aware embedding mechanism.

The Granularity-Aware Encoding Component: We study the impact of the granularity in the temporal patterns on the carbon intensity forecasting results. We examine four configurations on the granularity period g of the CFCG model:

- $CFCG_h : g \in \{hour\}$
- $CFCG_{h,d} : g \in \{hour, day\}$
- $CFCG_{h,w} : g \in \{hour, week\}$
- $CFCG_{h,d,w} : g \in \{hour, day, week\}$

The results are displayed in Fig. 6. $CFCG_{h,d,w}$ shows consistently better performance than the other configurations. $CFCG_{h,d,w}$ outperforms $CFCG_h$ by 11.07% (from 12.92 % to 14.35 %) in MAPE. This demonstrates that our design in integrating multiple time granularites into our CFCG model benefits the learning process. $CFCG_{h,d}$ is slightly better than $CFCG_{h,w}$ possibly due to finer-granularity. Overall, capturing temporal patterns in multiple granularities improves the performance of the model.

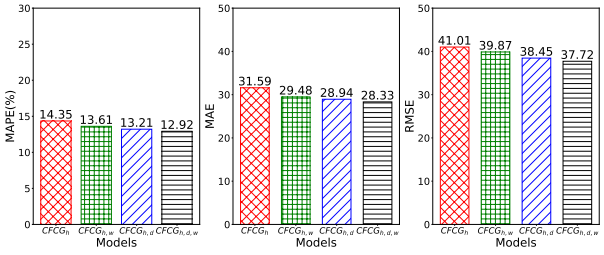

Figure 6: Effect of multi-granularity dynamics in terms of MAPE, MAE, and RMSE.

The Node-aware Embedding Mechanism: We study the impact of our node embedding mechanism, (i.e., we embed different types of nodes according to different rules) on the carbon intensity forecasting results. We compare *CFCG* with a simplified CFCG model $CFCG_{wn}$ by removing the node-aware embedding mechanism (i.e., removing the three rules). Fig. 7 shows the errors. We see that the averaged forecasting error with and without the node-aware embedding mechanism is comparable. This indicates that, on average, the level of noise is not high. However, we observe that in certain countries, the presence of the node-aware embedding mechanism can lead to a more significant impact. Fig. 8 shows that the node-aware embedding mechanism improved forecasting results in Sweden and the Czech Republic by 12.76% and 13.07%. When we investigate the data in detail, we see that the hourly electricity outflow of Sweden and the Czech Republic during the period 2019-2021 was 4185.95 MW and 2682.14 MW respectively, accounting for 23.21% and 29.29% of their electricity generation. Thus, the node-aware mechanism has a greater impact.

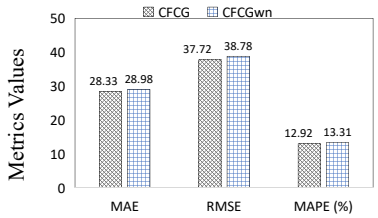

Figure 7: The forecasting error with and w/o node-aware embedding mechanism (NEM).

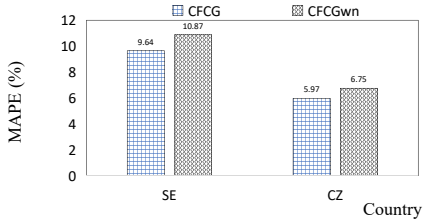

Figure 8: The forecasting error with and w/o node-aware embedding mechanism (NEM) on selected countries.

6.4 Explainable patterns learned (RQ3)

We attribute the performance improvements of CFCG to its ability to learn the spatial dependencies and temporal dependencies. We now visualize that CFCG has indeed learned these dependencies.

Spatial dependency learned. In Fig. 9 we illustrate the ground truth of the carbon intensity of the countries in the cross-border grids and the forecasting results in a spatial dimension. We illustrate the first two days in the testing data. We use color to show the ground truth, i.e., the darker the color, the greater the carbon intensity; and we use the size of a circle to show the forecasting results, i.e., the larger the circle, the greater the carbon intensity. We can see that the pattern of our forecasting results matches the ground truth in the spatial dimension.

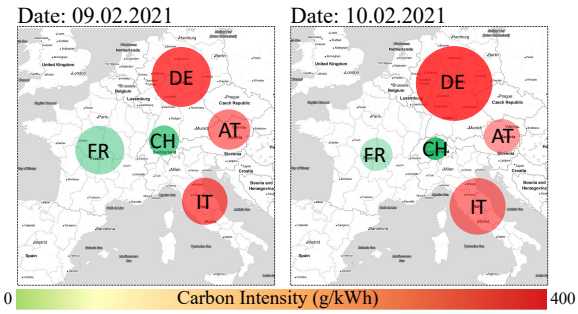

Figure 9: The spatial dependency learned by CFCG.

Temporal dependence learned. In Fig. 10 we illustrate the ground truth of the carbon intensity of the countries in the cross-border grids and the forecasting results in a temporal dimension. We show two randomly selected countries Sweden and Hungary. We can see that the pattern of our forecasting results matches the ground truth in the temporal dimension.

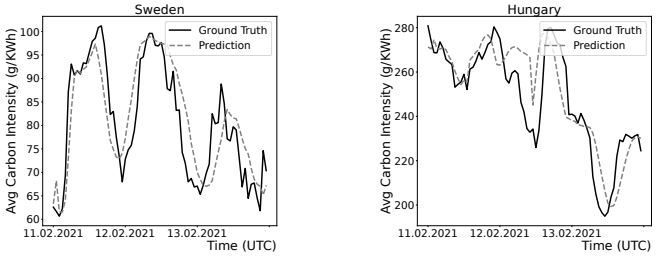

Figure 10: The temporal dependency learned by CFCG.

6.5 Performance Results under Alternative Ground Truths (RQ4)

As discussed previously, carbon intensity cannot be directly measured and different carbon intensity accounting methods are used to calculate the ground truth of carbon intensity from historical data. In our paper, we apply a direct coupling scheme in [27] to estimating the ground truth of carbon intensity. We now examine two alternative approaches to estimate the ground truth of the historical carbon intensity: the direct coupling approach [36] and the aggregate coupling approach [31]. We implement the two approaches to calculate two new ground truth datasets for carbon intensity. We show the results in Appendix Table 6). We see that the performance results remain the same across different ground truths. For example, CFCG achieves an average decrease of 19.80% (from 16.01% to 12.84%), 18.58% (from 15.77% to 12.84%), 21.65% (from 16.39% to 12.84%), 26.07% (from 17.37% to 12.84%), and 14.57%(from 15.03% to 12.84%) in MAPE compared to the DACF, TSBP, HMCF, CCAC, and CCAC-LSTM models based on Ground Truth 2. Intrinsically, our model is a learning model and it will not be affected by the ground truth of carbon intensity. This is confirmed in Appendix C.

7 CONCLUSION

In this paper, we studied day-ahead carbon intensity forecasting in the context of cross-border power grids. In cross-border power grids, the total carbon emissions of a local grid will not only carry the carbon emissions of its own grids (or its adjacent neighbor grids) but also carry the carbon emissions of the member grids in the cross-border grid. Current forecasting studies have yet to take this factor into their learning model. We showed that ignorance can lead to forecasting errors. We also showed that even we first estimate the carbon intensity of cross-border grids and use such history data to perform a learning using existing methods, e.g., LSTM, there can still be non-trivial errors. From the perspective of carbon intensity forecasting, cross-border power grids have both spatial and temporal dependencies in the carbon flow among member grids, and we need new designs to appropriately capture such dependencies. We developed a new learning model with embedded layers based on GNN and LSTM, learning the spatial and temporal dependencies, as well as designs of multi-periodic pattern encoding and node-aware embedding. We evaluated our model through the real-world data of the cross-border power grids in Europe with 28 member countries and the results showed that our model is effective in improving forecasting errors.

ACKNOWLEDGMENTS

The authors are indebted to the anonymous reviewers for their constructive comments; and their time and efforts guiding this paper into a better shape. This work is supported by RGC GRF 15210119, 15209220, 15200321, 15201322, ITF ITS/056/22MX, CRF C5018-20G of Hong Kong.

REFERENCES

[1] BW Ang, Peng Zhou, and LP Tay. 2011. Potential for reducing global carbon emissions from electricity production—A benchmarking analysis. *Energy Policy* 39, 5 (2011), 2482–2489.

[2] Beng Wah Ang and Bin Su. 2016. Carbon emission intensity in electricity production: A global analysis. *Energy Policy* 94 (2016), 56–63.

[3] Lasse F Wolff Anthony, Benjamin Kanding, and Raghavendra Selvan. 2020. Carbontracker: Tracking and predicting the carbon footprint of training deep learning models. *arXiv preprint arXiv:2007.03051* (2020).

[4] Francesco Asdrubali, Giorgio Baldinelli, Francesco D'Alessandro, and Flavio Scrucca. 2015. Life cycle assessment of electricity production from renewable energies: Review and results harmonization. *Renewable and Sustainable Energy Reviews* 42 (2015), 1113–1122.

[5] Heymi Bahar and Jehan Sauvage. 2013. Cross-border trade in electricity and the development of renewables-based electric power: lessons from Europe. (2013).

[6] Neeraj Dhanraj Bokde, Bo Tranberg, and Gorm Bruun Andresen. 2021. Short-term CO2 emissions forecasting based on decomposition approaches and its impact on electricity market scheduling. *Applied Energy* 281 (2021), 116061.

[7] Hans G Brauch. 2015. Environmental and Energy Security: Conceptual Evolution and Potential Applications to European Cross-Border Energy Supply Infrastructure. In *Environmental Security of the European Cross-Border Energy Supply Infrastructure*. Springer, 155–185.

[8] Art Diem, Cristina Quiroz, and TH Pechan. 2012. How to use eGRID for carbon footprinting electricity purchases in greenhouse gas emission inventories. *US Environmental Protection Agency* (2012), 2015–01.

[9] ENTSO-E. 2017. Electricity In Europe 2017, Statistics and Data. *https://www.entsoe.eu/publications/statistics-and-data/#electricity-in-europe* (2017).

[10] ENTSO-E. 2022. High-Level Report TYNDP 2022. *https://2022.entsos-tyndp-scenarios.eu/* (2022).

[11] Albert Gu, Caglar Gulcehre, Thomas Paine, Matt Hoffman, and Razvan Pascanu. 2020. Improving the gating mechanism of recurrent neural networks. In *International Conference on Machine Learning*. PMLR, 3800–3809.

[12] Edward Halawa, Geoffrey James, Xunpeng Shi, Novieta H Sari, and Rabindra Nepal. 2018. The prospect for an Australian–Asian power grid: A critical appraisal. *Energies* 11, 1 (2018), 200.

[13] Edgar G Hertwich and Richard Wood. 2018. The growing importance of scope 3 greenhouse gas emissions from industry. *Environmental Research Letters* 13, 10 (2018), 104013.

[14] Lion Hirth, Jonathan Mühlenpfordt, and Marisa Bulkeley. 2018. The ENTSO-E Transparency Platform–A review of Europe's most ambitious electricity data platform. *Applied energy* 225 (2018), 1054–1067.

[15] Sepp Hochreiter and Jürgen Schmidhuber. 1997. Long short-term memory. *Neural computation* 9, 8 (1997), 1735–1780.

[16] Hiroki Hondo. 2005. Life cycle GHG emission analysis of power generation systems: Japanese case. *Energy* 30, 11-12 (2005), 2042–2056.

[17] Paris IEA. 2022. Global Energy Review: CO2 Emissions in 2021. *https://www.iea.org/reports/global-energy-review-co2-emissions-in-2021-2* (2022).

[18] Kenneth Leerbeck, Peder Bacher, Rune Grønborg Junker, Goran Goranović, Olivier Corradi, Razgar Ebrahimy, Anna Tveit, and Henrik Madsen. 2020. Short-term forecasting of CO2 emission intensity in power grids by machine learning. *Applied Energy* 277 (2020), 115527.

[19] Gordon Lowry. 2018. Day-ahead forecasting of grid carbon intensity in support of heating, ventilation and air-conditioning plant demand response decision-making to reduce carbon emissions. *Building Services Engineering Research and Technology* 39, 6 (2018), 749–760.

[20] Diptyaroop Maji, Prashant Shenoy, and Ramesh K Sitaraman. 2022. CarbonCast: multi-day forecasting of grid carbon intensity. In *Proceedings of the 9th ACM International Conference on Systems for Energy-Efficient Buildings, Cities, and Transportation*. 198–207.

[21] Diptyaroop Maji, Ramesh K Sitaraman, and Prashant Shenoy. 2022. DACF: day-ahead carbon intensity forecasting of power grids using machine learning. In *Proceedings of the Thirteenth ACM International Conference on Future Energy Systems*. 188–192.

[22] Gregory J Miller, Kevin Novan, and Alan Jenn. 2022. Hourly accounting of carbon emissions from electricity consumption. *Environmental Research Letters* 17, 4 (2022), 044073.

[23] Divya Pandey, Madhoolika Agrawal, and Jai Shanker Pandey. 2011. Carbon footprint: current methods of estimation. *Environmental monitoring and assessment* 178 (2011), 135–160.

[24] Hans-Otto Pörtner, Debra C Roberts, H Adams, C Adler, P Aldunce, E Ali, R Ara Begum, R Betts, R Bezner Kerr, R Biesbroek, et al. 2022. Climate change 2022: Impacts, adaptation and vulnerability. *IPCC Sixth Assessment Report* (2022).

[25] Lidia Puka and Kacper Szulecki. 2014. The politics and economics of cross-border electricity infrastructure: A framework for analysis. *Energy Research & Social Science* 4 (2014), 124–134.

[26] O Pupo-Roncallo, J Campillo, D Ingham, L Ma, and M Pourkashanian. 2021. The role of energy storage and cross-border interconnections for increasing the flexibility of future power systems: The case of Colombia. *Smart Energy* 2 (2021), 100016.

[27] Shen Qu, Hongxia Wang, Sai Liang, Avi M Shapiro, Sanwong Suh, Seth Sheldon, Ory Zik, Hong Fang, and Ming Xu. 2017. A Quasi-Input-Output model to improve the estimation of emission factors for purchased electricity from interconnected grids. *Applied energy* 200 (2017), 249–259.

[28] Ana Radovanovic, Ross Koningstein, Ian Schneider, Bokan Chen, Alexandre Duarte, Binz Roy, Diyue Xiao, Maya Haridasan, Patrick Hung, Nick Care, et al. 2021. Carbon-aware computing for datacenters. *arXiv preprint arXiv:2106.11750* (2021).

[29] Ana Carolina Riekstin, Antoine Langevin, Thomas Dandres, Ghyslain Gagnon, and Mohamed Cheriet. 2018. Time series-based GHG emissions prediction for smart homes. *IEEE Transactions on Sustainable Computing* 5, 1 (2018), 134–146.

[30] Sebastian Ruder. 2016. An overview of gradient descent optimization algorithms. *arXiv preprint arXiv:1609.04747* (2016).

[31] Mirko Schäfer, Bo Tranberg, Dave Jones, and Anke Weidlich. 2020. Tracing carbon dioxide emissions in the European electricity markets. In *2020 17th International Conference on the European Energy Market (EEM)*. IEEE, 1–6.

[32] Prashant Shenoy. 2023. Energy-Efficiency versus Carbon-Efficiency: What's the difference? *ACM SIGENERGY Energy Informatics Review* 2, 4 (2023), 1–2.

[33] Bhupendra Kumar Singh. 2013. South Asia energy security: Challenges and opportunities. *Energy policy* 63 (2013), 458–468.

[34] Mary Elizabeth Sotos. 2015. GHG protocol scope 2 guidance. (2015).

[35] R Tomorrow. 2019. electricityMap. *https://www.electricitymap.org* (2019).

[36] Bo Tranberg, Olivier Corradi, Bruno Lajoie, Thomas Gibon, Iain Staffell, and Gorm Bruun Andresen. 2019. Real-time carbon accounting method for the European electricity markets. *Energy Strategy Reviews* 26 (2019), 100367.

[37] ENTSOE transparency platform. 2022. European association for the cooperation of transmission system operators. *Retrieved February 1, 2023 from https://transparency.entsoe.eu/* (2022).

[38] Philip Ulrich, Tobias Naegler, Lisa Becker, Ulrike Lehr, Sonja Simon, Claudia Sutardhio, and Anke Weidlich. 2022. Comparison of macroeconomic developments in ten scenarios of energy system transformation in Germany: National and regional results. *Energy, Sustainability and Society* 12, 1 (2022), 1–19.

[39] Jan Frederick Unnewehr, Anke Weidlich, Leonhard Gfüllner, and Mirko Schäfer. 2022. Open-data based carbon emission intensity signals for electricity generation in European countries–top down vs. bottom up approach. *Cleaner Energy Systems* 3 (2022), 100018.

[40] Petar Veličković, Guillem Cucurull, Arantxa Casanova, Adriana Romero, Pietro Lio, and Yoshua Bengio. 2017. Graph attention networks. *arXiv preprint arXiv:1710.10903* (2017).

[41] Jean Verseille and Konstantin Staschus. 2014. The mesh-up: ENTSO-E and European TSO cooperation in operations, planning, and R&D. *IEEE Power and Energy Magazine* 13, 1 (2014), 20–29.

[42] John Wamburu, Noman Bashir, David Irwin, and Prashant Shenoy. 2022. Data-driven decarbonization of residential heating systems. In *Proceedings of the 9th ACM International Conference on Systems for Energy-Efficient Buildings, Cities, and Transportation*. 49–58.

[43] Watttime. 2022. Watttime. *https://www.watttime.org/* (2022).

[44] Philipp Wiesner, Ilja Behnke, Dominik Scheinert, Kordian Gontarska, and Lauritz Thamsen. 2021. Let's wait awhile: how temporal workload shifting can reduce carbon emissions in the cloud. In *Proceedings of the 22nd International Middleware Conference*. 260–272.

[45] Priyantha Wijayatunga, Deb Chattopadhyay, and Prem N Fernando. 2015. Cross-border power trading in South Asia: A techno economic rationale. (2015).

[46] Mingzhou Xu, Derek F Wong, Baosong Yang, Yue Zhang, and Lidia S Chao. 2019. Leveraging local and global patterns for self-attention networks. In *Proceedings of the 57th Annual Meeting of the Association for Computational Linguistics*. 3069–3075.

[47] Xiyue Zhang, Chao Huang, Yong Xu, and Lianghao Xia. 2020. Spatial-temporal convolutional graph attention networks for citywide traffic flow forecasting. In *Proceedings of the 29th ACM international conference on information & knowledge management*. 1853–1862.

A APPENDIX A

Table 5: Country Abbreviations

Abbreviation	Country	Abbreviation	Country
AT	Austria	HU	Hungary
BE	Belgium	IE	Ireland
BG	Bulgaria	IT	Italy
CH	Switzerland	LT	Lithuania
CY	Cyprus	LV	Latvia
CZ	Czech	NL	Netherlands
DE	Germany	NO	Norway
DK	Denmark	PL	Poland
EE	Estonia	PT	Portugal
ES	Spain	RS	Serbia
FI	Finland	RO	Romania
FR	France	SE	Sweden
GR	Greece	SI	Slovenia
HR	Croatia	SK	Slovakia

B APPENDIX B

Carbon Intensity Accounting. Carbon intensity in a power grid cannot be directly measured. We now briefly present the detailed calculation of carbon intensity accounting. We follow [27] and [36]. Both apply the direct coupling scheme. In what follows, we first present the detailed calculation of [27]. Then we discuss [36], where different emission factors are used in different countries.

The total electricity of N regional power grids is represented as a 1 by N vector $\boldsymbol{x}$ whose element can be calculated by Eq. 12.

$$x_i = E_i + \sum_{j=1}^{N} f_{ji}^{e} \tag{12}$$

Where $\boldsymbol{E}$ is the 1 by N vector and E_i represents the electricity generation of grid i. $\boldsymbol{f^e}$ is an N by N matrix. The element f_{ij}^{e} of the matrix $\boldsymbol{f^e}$ refers to the exchange of electricity from grid i to grid j.

The amount of carbon emitted by all power grids is represented as a 1 by N vector $\boldsymbol{c^x}$. The element c_i^x of $\boldsymbol{c^x}$ refers to the total carbon emitted in the power grid i, including local generation amount of carbon emissions embodied in the importing of electricity, as in Eq. 13.

$$c_i^x = c_i^g + \sum_{j=1}^{N} b_{ji} c_j^x \tag{13}$$

where $\boldsymbol{B}$ is an N by N coefficient matrix, which captures the different shares of electricity exchanged in relation to total electricity. The element b_{ij} of $\boldsymbol{B}$ can be calculated by f_{ij}^{e}/x_i; c_i^g is the amount of carbon emissions generated by the local production of electricity in power grid i, which can be calculated using Eq. 14.

$$c_i^g = \sum_{m=1}^{n} E_i^k ef^k \tag{14}$$

where k denotes a specific energy source, ef^k is the emission factor of energy source k (see Table 1), and E_i^k is the electricity generated by source k in power grid i.

The Eq. 13 can be rearranged as Eq. 15, which is represented by vectors and matrices.

$$\boldsymbol{c^x} = \boldsymbol{c^g} + \boldsymbol{c^x B} = \boldsymbol{c^g}(\boldsymbol{I} - \boldsymbol{B})^{-1} \tag{15}$$

where $\boldsymbol{I}$ is an identity matrix.

Finally, the carbon intensity $\boldsymbol{ci}$ of cross-border power grids can be calculated using Eq. 16 according to the definition of the carbon intensity of electricity.

$$\boldsymbol{ci} = \boldsymbol{c^x}\hat{\boldsymbol{x}}^{-1} \tag{16}$$

where $\hat{\boldsymbol{x}}$ is the diagonal matrix of $\boldsymbol{x}$, and $\boldsymbol{ci}$ is a 1 by N vector that represents the carbon intensity of all N grids when electricity exchanges are taken into consideration.

In [36], it is observed that different generation technologies are used in different countries, leading to different emission factors for different countries. To capture this, Eq. 14 can be rewritten as

$$c_i^g = \sum_{m=1}^{n} E_i^k ef_i^k \tag{17}$$

where ef_i^k is the emission factor of energy source k in country i.

C APPENDIX C

Table 6: Performance results (in MAPE (%)) under three different carbon intensity accounting methods, representing three ground truth (Ground Truth GT1, GT2, GT3).

Methods	Ground Truth	Countries														
		AT	BE	BG	CH	CY	CZ	DE	DK	EE	ES	FI	FR	GR	HR	HU
DACF	GT1	24.07	19.61	5.53	59.06	**3.44**	8.00	11.31	25.20	25.33	14.95	10.21	18.77	**11.37**	14.43	9.10
	GT2	18.90	17.48	5.89	73.24	**2.12**	7.10	9.73	22.88	21.63	9.83	8.43	11.92	**7.90**	13.85	8.34
	GT3	17.96	16.15	4.86	74.44	**2.44**	6.08	8.92	21.82	21.71	8.90	8.25	10.93	**7.73**	12.13	8.14
TSBP	GT1	17.83	15.16	4.90	45.49	3.97	6.01	11.58	18.53	13.17	14.44	12.75	16.50	11.73	12.75	7.51
	GT2	17.91	15.21	4.89	48.98	3.21	5.72	11.65	18.56	14.24	14.20	12.81	16.34	11.68	12.97	7.65
	GT3	17.89	15.11	4.81	45.88	3.38	5.95	11.45	18.80	13.36	14.72	13.01	16.48	11.36	12.58	7.37
HMCF	GT1	16.59	15.86	5.87	46.86	3.65	6.12	12.77	18.38	13.87	14.17	11.54	16.95	13.21	12.43	7.51
	GT2	16.12	16.90	5.92	48.37	3.12	6.31	12.10	16.34	12.63	16.55	10.91	15.44	16.72	11.93	8.52
	GT3	18.47	14.55	5.32	45.88	2.66	6.03	13.10	14.55	13.88	15.21	9.24	13.21	14.55	10.88	7.51
CCAC	GT1	18.82	18.45	5.64	44.52	4.64	6.82	17.09	23.54	16.73	16.89	10.04	18.4	15.11	11.67	8.43
	GT2	23.90	17.88	8.99	45.31	5.17	8.23	22.29	31.40	17.76	16.55	12.26	21.36	15.80	16.13	8.54
	GT3	22.80	17.11	8.12	46.56	7.18	9.05	21.24	32.63	21.83	14.55	13.27	22.92	13.66	16.33	10.07
CCAC-LSTM	GT1	19.13	17.69	5.46	40.62	3.66	6.57	14.60	19.46	12.99	15.82	10.65	18.75	13.22	11.67	9.49
	GT2	18.38	16.94	5.74	47.89	3.91	5.84	11.81	18.66	12.24	15.10	9.94	17.96	12.51	10.92	8.78
	GT3	18.53	17.16	5.87	42.90	4.08	5.82	12.01	18.82	12.27	15.17	10.05	18.07	12.64	10.99	8.84
CFCG	GT1	**16.57**	**15.05**	**4.75**	**29.70**	3.9.	**5.97**	**10.91**	**16.94**	**12.48**	**12.67**	**8.86**	**14.74**	11.56	**10.34**	**7.06**
	GT2	**15.62**	**15.50**	**4.96**	**37.86**	4.22	**5.63**	**9.45**	**18.41**	**13.10**	**13.32**	**8.98**	**15.11**	10.91	**11.00**	**7.69**
	GT3	**15.82**	**15.59**	**4.49**	**37.85**	4.01	**5.86**	**9.50**	**18.22**	**12.91**	**13.28**	**8.21**	**14.98**	11.31	**10.53**	**7.26**

Methods	ground truth	Countries													
		IE	IT	LT	LV	NL	NO	PL	PT	RS	RO	SE	SI	SK	AVERAGE
DACF	GT1	**16.03**	8.50	46.95	24.66	7.11	20.81	6.57	23.88	7.38	9.42	12.89	31.09	16.17	17.57
	GT2	**12.98**	7.61	39.57	24.43	5.23	27.25	4.34	15.69	7.16	8.87	13.29	26.95	16.14	16.01
	GT3	**12.27**	7.75	35.97	22.49	5.31	28.74	4.14	14.64	6.20	4.86	12.30	25.97	15.20	15.24
TSBP	GT1	24.13	7.37	39.35	31.52	7.06	23.13	5.71	22.89	7.83	9.46	19.35	22.50	9.29	15.78
	GT2	24.05	7.05	38.89	32.43	6.09	23.45	4.81	22.12	7.94	8.47	19.42	22.63	8.26	15.77
	GT3	24.19	6.77	34.32	27.13	5.87	23.42	4.83	21.91	7.96	8.59	19.34	22.54	8.43	15.26
HMCF	GT1	24.65	7.48	41.50	30.96	7.08	23.54	5.79	22.76	11.41	9.57	19.05	25.42	9.37	16.22
	GT2	25.28	8.63	44.21	32.94	6.52	28.69	5.72	16.71	10.81	9.42	18.25	24.18	9.54	16.39
	GT3	23.45	7.21	40.55	31.54	5.79	26.74	5.05	19.25	9.75	8.65	17.88	24.56	8.89	15.51
CCAC	GT1	35.79	7.92	36.77	19.53	9.05	22.42	7.52	30.91	6.84	11.70	10.60	15.02	9.72	16.44
	GT2	38.83	9.77	30.29	14.59	9.27	25.12	9.71	29.53	6.24	16.30	9.80	14.40	9.06	17.37
	GT3	38.73	10.94	32.09	14.83	8.59	19.35	8.72	28.79	7.72	14.81	11.85	14.62	12.96	17.90
CCAC-LSTM	GT1	27.09	7.80	36.17	18.06	7.11	21.23	6.34	25.23	7.55	10.26	13.97	19.67	9.43	15.35
	GT2	26.35	7.06	37.41	19.35	6.37	20.51	5.56	24.48	6.83	9.52	13.25	18.90	8.67	15.03
	GT3	26.40	7.12	37.40	19.35	6.44	22.54	5.56	24.47	6.88	9.74	13.36	19.11	8.83	15.02
CFCG	GT1	22.66	**6.97**	**29.30**	**17.47**	**6.95**	**19.89**	**5.61**	**22.71**	**6.76**	**9.40**	**9.64**	**13.68**	**9.22**	**12.92**
	GT2	17.58	**6.94**	**31.16**	**18.25**	**5.94**	**20.21**	**4.36**	**15.39**	**7.07**	**8.37**	**9.54**	**14.90**	**8.10**	**12.84**
	GT3	17.19	**6.47**	**30.32**	**17.60**	**5.44**	**20.44**	**4.70**	**15.41**	**7.46**	**8.41**	**9.66**	**14.52**	**8.23**	**12.70**